Prediction of Pure Monopropellant Droplet Life Histories

G. M. FAETH*
Ordnance Research Laboratory, The Pennsylvania State University, University Park, Pa.

An earlier, approximate, burning rate theory is extended to yield heat and mass transfer rates of monopropellant droplets in the heat-up period as well as during steady burning at the wet bulb temperature. Experimental results were obtained to test the theoretical method by observing the life histories of supported ethyl nitrate and propylene glycol dinitrate droplets, under decomposition conditions, in the combustion products of a flat flame burner. The experiments were conducted with ambient gas temperatures in the range 1740–2640°K. Second-order global reaction rate parameters were found which correlated present steady burning rate data, as well as earlier tests conducted at higher pressures. Employing the measured reaction parameters, satisfactory predictions were made of droplet life histories for the two fuels considered in the study.

Nomenclature

A = dimensionless Arrhenius constant, Eq. (6)
B = Arrhenius constant
C_p, C_{p_d} = gas and liquid specific heat
d_0 = droplet diameter
D = effective binary diffusion coefficient
E = activation energy
k, k_d = gas and liquid thermal conductivity
K = burning rate constant, Eq. (24)
L = heat of vaporization
m = droplet mass
M = molecular weight
n = power in reaction expression
Nu = Nusselt number
q = heat of reaction
r = radial distance
R = universal gas constant
t = time
T = absolute temperature
v = dimensionless radial velocity = $v_r d_0/2D$
v_r = radial gas velocity
Y = fuel mass fraction
α_d = liquid thermal diffusivity
β = dimensionless radial distance = $d_0/2r$
Γ = dimensionless variable, Eq. (5)
δ = dimensionless reaction zone half width
ϵ = fuel mass flux fraction
θ = dimensionless temperature, Eq. (4)
θ_d = dimensionless temperature = $C_p T_0/q$
θ_a = dimensionless activation energy = E/RT_∞
ν = kinematic viscosity
ρ = gas density

Subscripts and superscripts

i = initial value
0 = at droplet surface
∞ = freestream conditions
I,II = outer and inner reaction zone boundary
* = center of reaction zone
$'$ = derivative with respect to β

Introduction

THERE have been numerous studies of monopropellant droplet burning at the wet bulb state,[1–3] i.e., the condition where all the energy reaching the droplet from the combustion zone is utilized for the heat of vaporization of the material evaporating from the surface of the droplet. However, in order to complete the computation of droplet life histories, which has been shown to be useful in estimating combustion chamber performance, it is also necessary to know transport rates as the droplet heats up from its injection temperature to the wet bulb temperature. This is particularly important at high pressures, where tests have shown that the heat-up period comprises the major part of the lifetime of a monopropellant droplet.[4] In the present study a method for the computation of monopropellant droplet life histories is developed and compared with experimental results obtained in an experiment which closely simulates combustion chamber conditions.

The present study extends earlier experimental work on monopropellant droplet combustion,[2,4] by suddenly subjecting a test droplet to the high temperature combustion products of a flat flame burner. This experimental approach avoids many of the previously encountered difficulties in data interpretation from furnace tests, which are subject to radiation effects and extremely nonadiabatic droplet burning to low ambient gas temperatures.[2,4]

A theoretical model is developed which extends the steady burning theory of Tarifa et. al.,[1] to include both the heat-up period of the droplet and the influence of convection. This model is used in conjunction with measured steady burning rates, from both the present study and Ref. 4, to obtain global rate controlling kinetics for the combustion of ethyl nitrate (EN) and propylene glycol dinitrate (PGDN) droplets. These results are then employed to compute droplet life histories for comparison with the experimental measurements. The influence of temperature gradients within the droplet on the results of the computations is also considered.

Theory

A major assumption of the analysis is a quasi-steady gas phase around the droplet. As used here, quasi-steady implies that the gas phase adjusts rapidly to the changing boundary conditions at the droplet surface, heat and mass transfer rates to the droplet are determined from a steady-state gas phase solution for the boundary conditions existing at each instant of time. The radius regression rate of the droplet was also neglected. The suitability of these assumptions for the present test conditions will be demonstrated later.

With respect to the gas phase, numerical integration has been employed to treat the developing combustion zone around a monopropellant droplet.[5] It was felt, however, that this method would be far too lengthy for application in the more complex theoretical models required for system

Received April 1, 1969; revision received July 31, 1969. This work was done under contract with the Naval Ordnance Systems Command, in conjunction with the Mechanical Engineering Department of The Pennsylvania State University. The author wishes to acknowledge useful discussions with D. R. Olson and R. H. Essenhigh during the course of the study.
* Associate Professor.

performance and instability analysis. Therefore, the following approximate analytical method was developed for the gas phase which only requires the relatively straightforward solution of a system of algebraic equations.

The gas phase model consists of a pure liquid monopropellant burning in an infinite atmosphere consisting of its combustion products. The fuel reacts in the gas phase via a one-step reaction characterized by global reaction rate parameters. The reaction path and specific rate constants are assumed to be unchanged during the lifetime of the droplet, i.e., there is no chemical induction period for the reaction.

It is assumed that the product species is insoluble in the liquid phase and only concentration diffusion is present. In the gas phase, all species are assumed to have identical properties, the Lewis number is taken to be unity and the gas properties and total pressure are assumed to be constant.

A film theory representation of convection was assumed since this approach has been successful for monopropellants, at least at low Reynolds numbers[5] (the only region where results are currently available for comparison). For the film theory approximation the actual flowfield around the droplet was replaced by a stagnant film of outer radius r_∞, where freestream conditions were attained. The outer radius was determined from Nusselt number correlations, in the absence of mass transfer and chemical reaction, for the specified flow conditions.[5]

With these assumptions, the gas phase equations of conservation of mass, energy and species may be readily obtained from the more general equations given by Williams.[6] Assuming an Arrhenius reaction rate expression, the dimensionless form of these equations is as follows:

$$d/d\beta(d\Gamma/d\beta + v_0\Gamma) = 0 \tag{1}$$

$$dY/d\beta + v_0(Y - \epsilon) = 0 \tag{2}$$

$$\frac{d\epsilon}{d\beta} = \frac{AY^n}{v_0\beta^4} \exp\left\{\frac{-\theta_a(\theta_\infty - \theta)}{\theta + \theta_d}\right\} \tag{3}$$

where

$$\theta = (C_p/q)(T - T_0) \tag{4}$$

$$\Gamma = (\theta + Y - Y_0)/(\theta_\infty - Y_0) \tag{5}$$

$$A = (Bd_0^2\rho^{n-1}/4D) \exp\{-E/RT_\infty\} \tag{6}$$

The boundary conditions on these equations are,

$$\begin{aligned} &Y = Y_0,\ \Gamma = 0,\ \epsilon = 1; \qquad \beta = 1 \\ &Y = \epsilon = 0,\ \Gamma = 1; \qquad \beta = \beta_\infty \end{aligned} \tag{7}$$

The solution of Eq. (1) may be obtained immediately, as follows:

$$\Gamma = \{\exp[v_0(1 - \beta)] - 1\}/\{\exp[v_0(1 - \beta_\infty)] - 1\} \tag{8}$$

The remainder of the solution follows the approximate analytical method first introduced by Tarifa et. al.[1] With this method, the reaction is limited to a zone of width 2δ (in the β coordinate system), centered at a flame position, β^*. Within this region, the rate of change of fuel mass flux fraction, $\epsilon' = d\epsilon/d\beta$, is assumed to have the following form

$$\epsilon' = \epsilon'^*[1 - abs(\beta - \beta^*)]/\delta$$

with $\epsilon' = 0$, elsewhere. The definition of the reaction approximation is completed by requiring that ϵ' satisfy Eq. (3) at β^*,

$$\epsilon'^* = (AY^{*n}/v_0\beta^{*4}) \exp\{[-\theta_a(\theta_\infty - \theta^*)]/[\theta^* + \theta_d]\} \tag{9}$$

and also

$$d^2\epsilon/d\beta^2 = 0, \qquad \beta = \beta^* \tag{10}$$

Taking the derivative of Eq. (3), substituting this into Eq. (10) and simplifying through Eq. (8) yields,

$$\frac{4}{v_0\beta^*} = \frac{n(\frac{1}{2} - Y^*)}{Y^*} - \frac{\theta_a(\theta_\infty + \theta_d)}{(\theta^* + \theta_d)^2} \times \left[\frac{(Y_0 - \theta_\infty)}{v_0}\Gamma'^* + \frac{1}{2} - Y^*\right] \tag{11}$$

In order for the reaction to be completed within the reaction zone, the following must also be true,

$$\epsilon'^*\delta = 1 \tag{12}$$

With this approximation, Eqs. (2) and (3) may be integrated to yield Y and ϵ in the various regions of the boundary layer. Continuity of Y at β^* then yields the following two equations,

$$Y^* = (\epsilon'^*/2v_0^2)\{(v_0\delta - 1)^2 + 1 - 2\exp(-v_0\delta)\} \tag{13}$$

$$Y^* = 1 - (1 - Y_0)\exp[v_0(1 - \beta^*)] - (\epsilon'^{*2}/2v_0^2) \times \{(v_0\delta + 1)^2 + 1 - 2\exp(v_0\delta)\} \tag{14}$$

The outer boundary, β_∞, may be obtained from the known flow conditions as discussed in Ref. 5. Evaluating Eq. (8) at β^*, along with Eqs. (9 and 11–14) provides six algebraic equations to solve for the remaining unknowns v_0, β^*, θ^*, Y^*, ϵ'^*, and δ. For the case where $v_0\delta \ll 1$, Eqs. (13) and (14) can be simplified to yield

$$v_0 = [-1/(1 - \beta^*)]\ln(1 - Y_0) \tag{15}$$

and

$$Y^* = v_0\delta/6 \tag{16}$$

In the present calculations, Eqs. (15) and (16) were employed for the solution. The calculations were performed by iteration, with β^* being varied until the correct value of A was obtained from Eq. (9).

The accuracy of this solution at the wet bulb state has been considered in Ref. 7. The results of Ref. 5 were employed to test the analysis for the heat-up period. Differences in heat and mass transfer rates on the order of 5% were encountered between the two solutions over the range of variables available from the numerical computations ($0 < A < 10^5$, $6 < \theta_a < 12$, $0 < Y_0 < 0.9$, θ_a on the order of unity and the Reynolds number less than unity). The largest errors were encountered for the smallest values of θ_a. In view of the uncertainties in properties and reaction parameters, it appears that this approximation would be adequate in many situations (although it should be applied with care for parameter values outside the above ranges).

Two models of the temperature distribution within the droplet were employed for the computation of droplet life histories. In the first (infinite thermal conductivity model), the droplet temperature was assumed to be uniform at each instant of time. Under this assumption, for constant liquid properties, the equations of conservation of mass and energy of the droplet become

$$dm/dt = -2\pi d_0\rho D v_0 \tag{17}$$

$$\frac{dT_0}{dt} = \frac{\pi d_0\rho D}{mC_{pd}}[C_p(T_\infty - T_0)Nu - 2v_0L] \tag{18}$$

where

$$Nu = \frac{2v_0}{\theta_\infty}\left\{\frac{(1 - Y_0)\exp[v_0(1 - \beta_\infty)] + \theta_\infty - 1}{\exp[v_0(1 - \beta_\infty)] - 1}\right\} \tag{19}$$

Equations (17) and (18) were numerically integrated, with the gas phase solution yielding v_0 and Nu, employing the Hamming predictor-corrector method. The vapor pressure curve of the droplet material provided the required relationship between Y_0 and T_0.

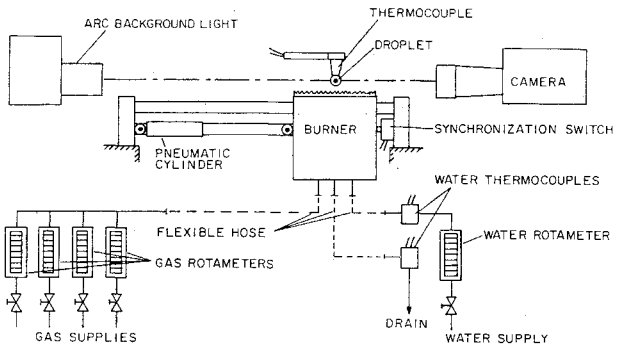

Fig. 1 Layout of experimental apparatus.

The second model considered the actual temperature distribution within the droplet under the assumption that there was no circulation of the droplet liquid (finite conductivity model). The equation of conservation of mass is unchanged in this case. The equation of conservation of energy within the droplet becomes

$$\partial T/\partial t = (\alpha_d/r^2)(\partial/\partial r)(r^2\partial T/\partial r) \quad (20)$$

with the following boundary condition at the surface of the droplet

$$\partial T/\partial r = (\rho D/k_d d_0)[C_p(T_\infty - T)Nu - 2v_0 L],\ r = r_0 \quad (21)$$

Equations (17, 20, and 21) were integrated numerically, employing the gas phase solution for Nu and v_0. The specific computational procedures used in the calculations may be found in Ref. 14.

Apparatus

A sketch of the experimental apparatus is shown in Fig. 1. The flat flame burner was mounted on rails so that it could be rapidly moved under the droplet location and returned to its initial position at the end of burning with a solenoid valve actuated pneumatic cylinder. The burner face was 5 cm in diam and in the test position (illustrated in Fig. 1) the droplet was 1 cm above the center of the burner. The time between the droplet first entering the burner flame and the burner coming to rest in the test position was on the order of 10 msec.

The construction of the flat flame burner was similar to the one described by Friedman and Macek.[8] The burner was operated with various mixtures of carbon monoxide, hydrogen, oxygen and nitrogen (commercial grade). The flow of these gases was measured by rotameters which, in turn, were calibrated with a wet test meter. The heat loss from the flat flame to the burner surface was determined by measuring the temperature rise and flow rate of the burner cooling water. The temperature and composition of the burned gas flowing around the droplet was determined from thermochemical calculations accounting for all relevant dissociation reactions. The thermochemical properties for these calculations were taken from the JANAF tables.[9]

For burning rate measurements, the droplet was mounted from a quartz filament having a diameter of approximately 100μ with a 500μ diam bead at one end to support the droplet. In tests where droplet temperatures were measured, the droplet was supported from a 500μ diam sauereisen cement bead containing a chromel-alumel thermocouple junction. The thermocouple was constructed from 25μ wires in order to reduce conduction errors from the hot gas environment. The thermocouple junction was located at the surface of the cement bead, toward the center of the droplet.

Droplet diameters were measured from shadowgraphs recorded by a 16 mm cine camera operating at speeds on the order of 100 pictures per sec. The elliptical shape of the droplet was corrected to a sphere of equal volume.[4] The temperature and film records were synchronized by a switch closure as the droplet entered the burner flame.

Evaporation Tests

In order to establish calculation procedures for the selection of the average properties employed in the analysis, preliminary theoretical and experimental comparisons were made for the case of evaporation without reaction. Aside from neglecting decomposition in the boundary layer of the droplet, the analysis of the evaporation process was done under the same general assumptions as for the reactive case. The specific transport equations employed for the computed results are as follows

$$v_0 = [-\ln(1 - Y_0)]/(1 - \beta_\infty) \quad (22)$$

$$Nu = 2v_0(1 - Y_0)/Y_0 \quad (23)$$

Water was chosen as the test material because of its relatively high thermal stability at the temperature levels of the present study. The property values employed in the calculations are shown in Table 1. The gas phase properties were computed for the arithmetic average temperature and composition at the wet bulb state. An exception to this was the kinematic viscosity, which is employed in the Reynolds number to evaluate β_∞.[5] Other work in this laboratory has indicated that the use of the ambient composition at the average temperature yields a better estimation of the influence of convection—particularly for the heavier hydrocarbons. Therefore, this latter procedure was employed for the present study. The binary diffusivity was selected to make the Lewis number unity.

A typical comparison between theory and experiment is shown in Fig. 2. The results of the finite conductivity model indicate that there are large temperature gradients within the droplet during the beginning of the lifetime. This was reflected experimentally by difficulties in obtaining reproducible temperature traces in this region due to variations in thermocouple position within the droplet. However, temperature gradient effects did not have a large influence on the predicted droplet diameter variation for these conditions. Since the agreement between theory and experiment was adequate, an analogous method was employed for determining physical properties for the monopropellants.

Influence of Oxygen on Burning Rates

Previous investigations have shown that droplet burning rates of fuel rich monopropellants are sensitive to ambient oxygen concentration.[2,4] With the present experimental technique it is impossible to achieve a completely oxygen free ambient environment around the droplet due to dissociation of the reaction products of the burner. Since it was desired to simulate pure decomposition conditions, the first series of tests were run with various ambient oxygen concentrations in order to evaluate the influence of this effect.

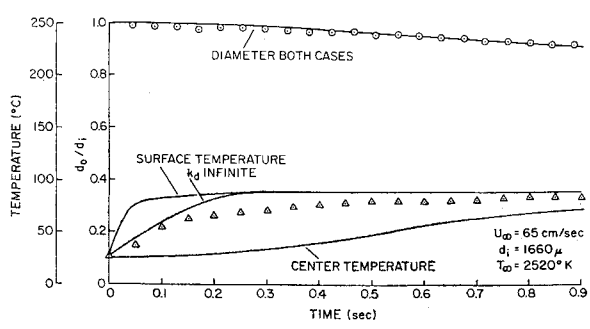

Fig. 2 Predicted and measured water droplet life history.

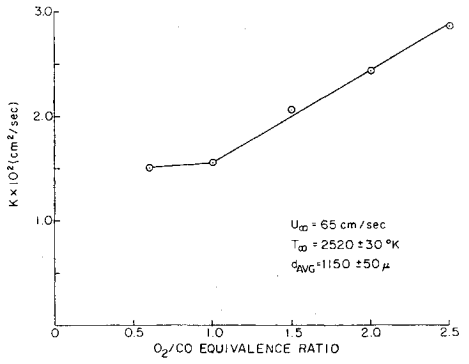

Fig. 3 Burning rate constant of EN for various burner equivalence ratios.

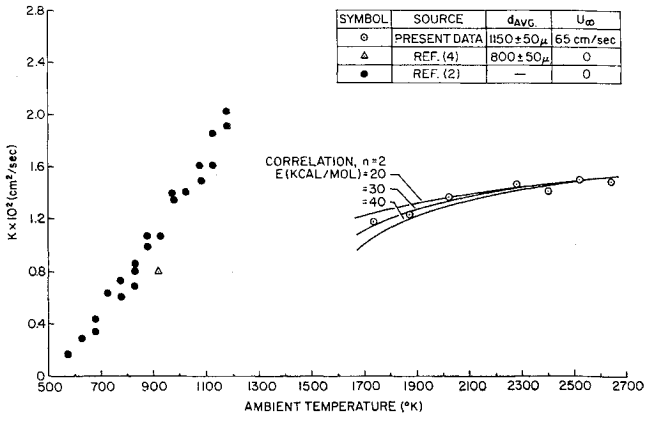

Fig. 4 Burning rate constant of EN at various ambient temperatures.

The results of these tests for EN with a constant ambient gas velocity and temperature are shown in Fig. 3. The burning rate constant was measured during the steady burning period of the droplet. It was defined on a diameter basis as follows

$$K = -dd_0^2/dt \tag{24}$$

The burning rate constant was employed to characterize the data since plots of diameter squared with respect to time gave reasonably straight lines, even though this parameter is not entirely suitable for monopropellant combustion.[4] The points plotted on the figure represent averages of six tests.

Increasing oxygen concentrations are seen to have a strong influence on burning rates. In view of the high ambient temperatures of these tests, it would appear that the increased burning rate is due either to direct kinetic participation of the oxygen in the decomposition process or the presence of a diffusion flame between the decomposition zone and the outer edge of the boundary layer. In either case, it appears that the approach suggested in Ref. 15, for treating the combustion of a monopropellant burning in an oxidizing atmosphere, would have to be modified in order to correlate the results observed in these tests.

Increasing the concentration of carbon monoxide in the ambient gas had very little effect. In fact, most of the slight reduction in burning rate, for equivalence ratios less than unity, probably can be attributed to the reduction in oxygen concentration through the suppression of the dissociation of carbon dioxide due to excess carbon monoxide in the combustion gas (for an equivalence ratio of unity the ambient oxygen concentration through dissociation is approximately 4% by volume, at an equivalence ratio of 0.6 the concentration is approximately 0.4%). Similarly, the concentration of hydrogen in the flat flame burner did not cause a significant effect on the droplet burning rates.

As a result of these tests, the remainder of the experimental work was conducted with a fuel-rich mixture reacted in the flat flame burner. The conditions of all the results to be reported were such that the ambient oxygen concentration was less than $1\frac{1}{2}\%$ by volume, through dissociation.

Influence of Temperature on Burning Rates

Steady-state burning rate measurements were made at various ambient temperatures with a constant ambient gas velocity. The test results for EN are shown in Fig. 4, along with earlier results obtained in furnace tests at lower ambient temperatures from Refs. 2 and 4. The present test points represent averages of six tests, the points from the earlier work represent single tests. The temperature range of the present experiments was reasonably broad, spanning 900°C. The test conditions were limited at high temperatures due to dissociation yielding excessive oxygen concentrations and at low temperatures by blow-off of the burner.

It is disturbing to note that burning rates for the furnace tests are higher than the present results even though the ambient gas temperatures are far lower. It is felt that radiation from the furnace walls might provide the explanation of this result. For droplets of these sizes, furnace wall radiation contributed significantly to droplet evaporation at temperatures above 800°K, at atmospheric pressure.[4] In the present tests, only radiation from the ambient gas to the droplet must be considered, and this is of little consequence due to low gas densities and short path lengths. (Note that due to small droplet sizes and high rates of convection, particularly at elevated pressures, wall radiation does not ordinarily play a large role in droplet evaporation in combustion chambers.)[16]

In order to proceed with the droplet lifetime calculations, the present burning rate data were employed to obtain the relevant global reaction rate parameters in conjunction with the theory. The property values employed in these calculations are shown in Table 1. The heat of reaction was chosen to yield the correct adiabatic flame temperature, computed thermochemically and allowing for dissociation, for the as-

Table 1 Properties employed in the computations[a]

Property	Units	Water	EN	PGDN
k_d	cal/sec cm°K	1.6×10^{-3}	4.0×10^{-4}	3.9×10^{-4}
ρ_d	g/cm³	1.0	1.11	1.39
C_{pd}	cal/g°K	1.0	0.440	0.415
L	cal/g	590	95.5	90.5
ρ	g/cm³	2.47×10^{-4}	4.87×10^{-4}	7.65×10^{-4}
ν	cm²/sec	1.86	1.86	1.86
C_p	cal/g °K	0.617	0.545	0.480
k	cal/cm sec°K	2.66×10^{-4}	2.2×10^{-4}	2.2×10^{-4}
D	cm²/sec	1.75	0.83	0.60
q	cal/g	...	975	1280
M	g/gmol	30.2	61.7	97

[a] Atmospheric pressure; density of gas, etc., corrected under ideal gas assumption for other pressures.

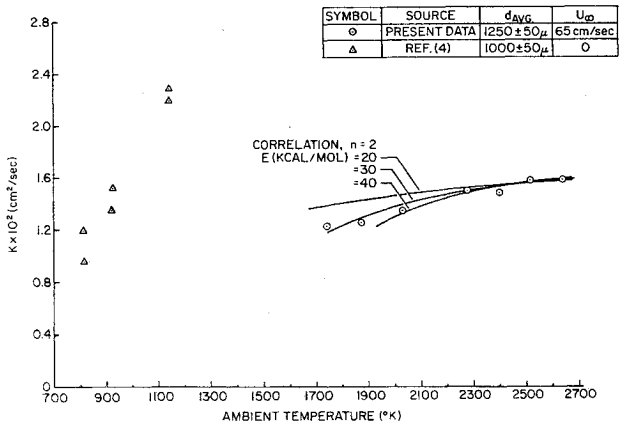

Fig. 5 Burning rate constant of PGDN at various ambient temperatures.

sumed value of C_p.[5] The computed adiabatic flame temperatures were 1910°K for EN and 2790°K for PGDN, for an initial liquid temperature of 298°K.

In making the reaction rate correlation, various activation energies and both first and second-order controlling reactions were considered. The procedure was to select the Arrhenius constant for a given reaction order and activation energy so that the theory matched the experimental results at some temperature. The theoretical burning rate was then computed at other temperatures over the test range and compared with the experimental results.

A comparison of this type of correlation for a second order reaction is shown in Fig. 4. It appears that the computed variation of the burning rate is relatively insensitive to the assumed value of the activation energy over the range of the tests. This implies that while an activation energy can be chosen which correlates droplet burning rates reasonably well, it is unlikely that an activation energy selected for this purpose would be useful in another context.

Because of a discontinuous jump in the burning rate at lower ambient temperatures,[1] the correlation should not be employed at ambient temperatures much below the range indicated on the figure, at atmospheric pressure. At higher pressures, solutions are obtained over a broader ambient temperature range, as will be discussed later.

Figure 5 shows a similar plot of burning rate as a function of temperature for PGDN. The general characteristics of

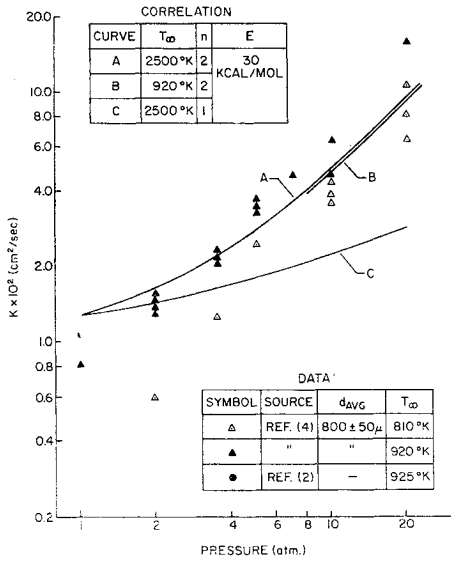

Fig. 6 Correlation of the pressure dependence of the burning rate constant of EN.

Table 2 Correlation of global reaction rate parameters

Fuel	n	E Kcal/gmol	B	
EN	1	30	2.64×10^8	sec^{-1}
EN[a]	2	30	1.22×10^{10}	liters/gmol sec
PGDN	1	30	2.34×10^7	sec^{-1}
PGDN[a]	2	30	9.23×10^8	liters/gmol sec

[a] Recommended correlation.

this plot are the same as for EN. The sensitivity of the correlation to the assumed value of the activation energy is somewhat greater for PGDN than was the case for EN, but still a rather broad range of activation energies could adequately represent the data.

The chemical parameters resulting from the best fit of the experimental data for first and second order reactions are shown in Table 2. If the controlling reaction event was the initial breakdown of the molecule, first order kinetics would be expected.[10] Examination of Table 2, however, indicates that the pre-exponential factors from the present correlation, for first order kinetics, are almost seven orders of magnitude smaller than the values reported for the decomposition of these molecules.[10-12] Thus it appears that the initial decomposition of the molecules is far too fast to exert control of the over-all reaction for ambient temperature levels on the order of combustion chamber temperatures. In contrast to this, the second-order pre-exponential factors, in Table 2, appear to have reasonable magnitudes when compared to other typical values in the literature.[13]

Influence of Pressure on Burning Rates

Further insight into the correct order for the correlating reaction scheme may be obtained by considering the experimental results of Ref. 4. While the measurements of atmospheric pressure can be criticized as before, at higher pressures most of these objections disappear. With higher burning rates at high pressures, the contribution of radiation from the furnace walls (which is relatively independent of pressure) to the total gasification rate of the droplet, becomes a progressively smaller percentage of the total as the pressure is increased.

Figures 6 and 7 show a comparison of the present correlations (allowing for natural convection) with the furnace test results. Curves A and C were constructed for rather high ambient temperatures in order to avoid the previously discussed discontinuous region at low pressures and low ambient temperatures. Curve B, constructed for the ambient temperature of the furnace tests, indicates only a small influence

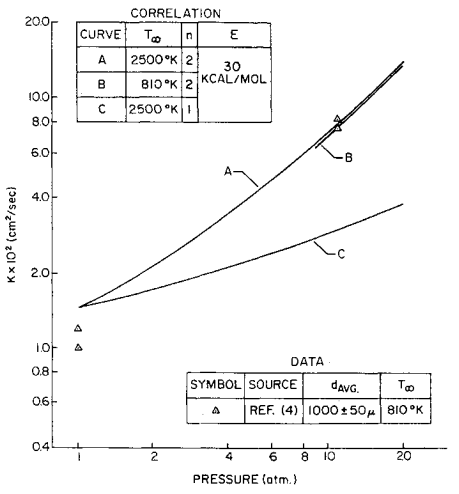

Fig. 7 Correlation of the pressure dependence of the burning rate constant of PGDN.

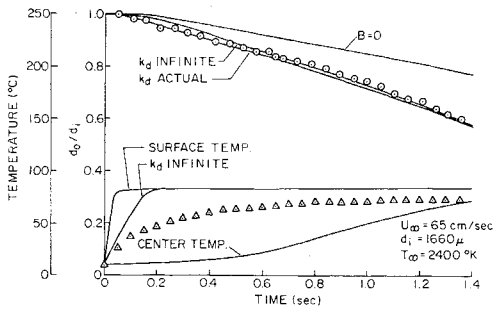

Fig. 8 Predicted and measured EN droplet life history.

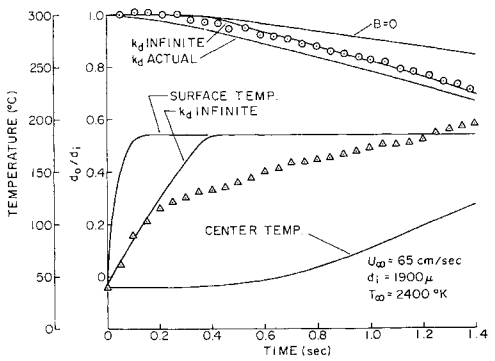

Fig. 9 Predicted and measured PGDN droplet life history.

of ambient temperature on the correlation at the higher pressures in the test range.

These comparisons clearly indicate that the second-order scheme gives the best correlation of the trends in burning rate with increasing pressure. For the EN results, there appears to be a greater influence of ambient temperature on the measured burning rates than is shown by the correlation, however, considering the scatter of data, this effect is not well established at the higher pressures. It also appears that the second-order correlation gives a reasonably good representation of the magnitude of the furnace data at higher pressures, where the experimental difficulties of this technique are minimized (admittedly, the target is rather large in the case of EN).

Droplet Life Histories

Utilizing the second-order global reaction rate parameters from the burning rate measurements, the theory was employed to compute droplet life histories for comparison with the experimental results. Droplets having initial diameters in the range 1000–2000μ were employed in these comparisons. A typical comparison for a large EN droplet is shown in Fig. 8.

The differences between the diameter variations predicted by the finite and infinite conductivity models is not very large for these conditions and both models agree reasonably well with the measurements. The theoretical curve plotted for negligible reaction, $B = 0$, provides an indication of the influence of chemical reaction on the gasification process. Because of the rapid increase in burning rate with pressure, indicated in Figure 6, the differences between the reactive and nonreactive solutions would be much greater at higher pressures. For completeness, the temperature results are also shown on the figure, but it is apparent that the presence of temperature gradients within the droplet precludes any definite conclusions based on these data.

A typical life history for PGDN is shown in Fig. 9. The more extended heat-up period for this less volatile fuel results in greater differences between the diameter predictions of the two models. The finite conductivity model yields more rapid evaporation in the early stages of the lifetime since the surface temperature reaches temperature levels near the wet bulb state more rapidly. A compensating feature of this effect is a somewhat slower gasification rate in the latter portions of the lifetime, for the finite conductivity model, due to continued heat transfer toward the center of the droplet.

While the agreement between the measured and predicted droplet life histories shown in Figs. 8 and 9 is reasonably satisfactory, it must be emphasized that this test of the heat-up theory has not been very severe. For the present test conditions, the heat-up period of the droplet still represents a fairly small percentage of the total lifetime and errors in transport rate predictions during heat-up could easily go undetected. Additional experimental work with high temperature ambient environments at higher pressures, where the heat-up period is a much larger percentage of the total lifetime, is required in order to provide a more adequate test of the theoretical method.

The applicability of the quasi-steady assumption may be tested by comparing the droplet lifetime with the characteristic time of transient gas phase processes. Williams[17] has suggested the parameter $d_0^2/(4D)$ as a characteristic time for a convection free environment. Employing the properties of Table 1, this parameter is on the order of one thousand times smaller than the droplet lifetimes observed during the investigation. This indicates relatively rapid adjustment of the gas phase to changes at the droplet and substantiates the use of the quasi-steady assumption in the analysis of the present test data. Neglecting the effect of finite radius regression rate is also justified for the present conditions since the liquid density is much greater than the density of the gas phase.[17]

Conclusions

The experimental approach employed in the present study has significant advantages over the earlier furnace tests due to the elimination of radiation and the provision of gas temperatures representative of combustion chamber conditions. The second-order global reaction rate parameters obtained from the present study were found to be in reasonably good agreement with the results of furnace tests at high pressures where many of the experimental uncertainties of this latter procedure are reduced. The extension of Tarifa's steady burning analysis to the heat-up period appears to provide a method suitable for the computation of monopropellant life histories, with a reasonable expenditure of computer time. The method is continuous in that it does not require the specification of a time of ignition. It is emphasized, however, that the test of this method at atmospheric pressure has not been very severe, pointing to the need for further data at high pressures, with ambient temperatures representative of combustion chamber conditions. Furthermore, the approximate method should be used with care for parameter values outside the range considered in the present investigation.

References

[1] Tarifa, C. S., del Notario, P. P., and Moreno, F. G., "Combustion of Liquid Monopropellants and Bipropellants in Droplets," *Eighth Symposium (International) on Combustion*, Williams and Wilkins, Baltimore, Md., 1962, pp. 1035–1056.

[2] del Notario, P. P. and Tarifa, C. S., "An Experimental Investigation on the Combustion of Monopropellant Droplets," TN 59-628, Jan. 1959, Air Force Office of Scientific Research.

[3] Williams, F. A., "Theory of the Burning of Monopropellant Droplets," *Combustion and Flame*, Vol. 3, No. 4, Dec. 1959, pp. 529–543.

[4] Faeth, G. M., Karhan, B. L., and Yanyecic, G. A., "Ignition and Combustion of Monopropellant Droplets," *AIAA Journal*, Vol. 6, No. 4, April 1968, pp. 684–689.

[5] Faeth, G. M., "Flame Zone Development of Monopropellant Droplets," *Combustion and Flame*, Vol. 12, No. 5, Oct. 1968, pp. 411–416.

[6] Williams, F. A., *Combustion Theory*, Addison-Wesley, Reading, Mass., 1965, Chap. 1.

[7] Tarifa, C. S. and Larrazabel, J. M. S., "Combustion of Monopropellant Droplets," TN 57-671, July 1957, Air Force Office of Scientific Research.

[8] Freidman, R. and Macek, A., "Ignition and Combustion of Aluminum Particles in Hot Gases," *Combustion and Flame*, Vol. 6, No. 1, March 1962, pp. 9–19.

[9] Jones, W. H. (Chairman), "JANAF Thermochemical Tables," Dow Chemical Co., Midland, Mich.

[10] Phillips, L., "Thermal Decomposition of Organic Nitrates," *Nature*, Vol. 160, No. 4074, Nov. 1947, pp. 753–754.

[11] Levy, J. B., "The Thermal Decomposition of Nitrate Esters, I. Ethyl Nitrate," *The Journal of the American Chemical Society*, Vol. 76, June 1954, pp. 3254–3257.

[12] Adams, G. K. and Bawn, C. E. H., "Homogeneous Decomposition of Ethyl Nitrate," *Transactions of the Faraday Society*, Vol. 45, 1949, pp. 484–499.

[13] Benson, S. W., *The Foundations of Chemical Kinetics*, McGraw-Hill, New York, 1960, Chap. 12.

[14] Faeth, G. M., "The Kinetics of Droplet Ignition in a Quiescent Air Environment," Ph.D. thesis, 1964, The Pennsylvania State University, University Park, Pa.

[15] Beltran, M. R. et. al., "Analysis of Liquid Rocket Engine Combustion Instability," TR-65-254, Jan. 1966, Air Force Rocket Propulsion Lab.

[16] Hottel, H. C., Williams, G. C., and Simpson, H. C., "Combustion of Droplets of Heavy Liquid Fuels," *Fifth Symposium (International) on Combustion*, Reinhold, New York, 1955, pp. 101–129.

[17] Williams, F. A., "On the Assumptions Underlying Droplet Vaporization and Combustion Theories," *Journal of Chemical Physics*, Vol. 33, No. 1, July 1960, pp. 133–144.

JULY 1970 AIAA JOURNAL VOL. 8, NO. 7

Ignition and Surface Temperatures of Double Base Propellants at Low Pressure: I. Thermocouple Measurements

N. P. Suh,* C. L. Tsai,† C. L. Thompson Jr.†, and J. S. Moore†
University of South Carolina, Columbia, S.C.

The autoignition, ignition, and surface temperatures of M-2 double base propellant were determined at low pressures. The autoignition temperature is defined to be equal to the initial temperature of the propellant at which the burning rate approaches infinity, which was found to be 145°C for M-2 propellant. The temperature at which a noticeable self-sustaining deflagration of the propellant first occurs (ignition temperature) was determined by imbedding a thermocouple at one end of the propellant specimen subject to a radiant flux. At 1 psia, the ignition temperature was found to be 214°C. The surface temperatures of the double-base propellant for steady-state burning were determined by imbedded thermocouple wires of various sizes, at pressures of 5, 10, and 15 psia. These thermocouple measurements were corrected by using a theoretical model of the thermocouple response characteristics. The correct surface temperature was determined by checking whether an assumed value predicted the experimentally measured bead temperatures of ½-, 1-, 2-, and 3-mil thermocouple wires. The emergence of the thermocouple bead from the solid into the gas phase was determined by high-speed motion pictures and is invariably associated with a plateau in the oscillograph recording of the temperature profile. The surface temperature predicted at these low pressures is about 300°C.

Nomenclature

A = surface area
B = $\rho C_p r/k$ of propellant
C_1, C_2, etc. = parameters defined in the text
C_p = specific heat of propellant at constant pressure
C_{pw} = specific heat of thermocouple wire at constant pressure
D = diameter of thermocouple bead
h = heat-transfer coefficient
k = thermal conductivity (of propellant, when used without a subscript)
L = length of thermocouple wire imbedded in propellant
P = length of thermocouple wire periphery
Q_{lead} = heat loss rate through thermocouple lead wires
r = burning rate
R = radius of thermocouple wire
t = time
T = temperature
V = volume
X, Y = coordinates defined in the text
ρ = density (of propellant, when used without a subscript)
α = angle between lead wire and axis of propellant

Subscripts

o = initial condition
B = thermocouple bead
p = propellant
s = burning surface
w = thermocouple wire

Received May 5, 1969; revision received January 13, 1970. Supported by Pitcatinny Arsenal through the Army Research Office-Durham, Grant DA-ARO-D-31-124-61029 (Monitor, Charles Lenchitz).

* Associate Professor, College of Engineering; presently Associate Professor, Department of Mechanical Engineering, Massachusetts Institute of Technology.

† Research Assistant, College of Engineering.